

Design of tangential viewing phase contrast imaging for turbulence measurements in JT-60SA

87

Articles you may be interested in

22

21

21

20

77



Nanopositioning Systems **Micropositioning** **AFM & SPM** **Single molecule imaging**

The image displays four categories of scientific instruments from Mad City Labs Inc. (MCL). From left to right: 1. Nanopositioning Systems, shown as a light-colored square platform with a central square hole. 2. Micropositioning, shown as a dark, rectangular block with several small protrusions on its top surface. 3. AFM & SPM, shown as a small, light-colored rectangular device with a striped pattern on its top surface. 4. Single molecule imaging, shown as a complex, dark-colored mechanical assembly with a camera or detector unit on the right.

Design of tangential viewing phase contrast imaging for turbulence measurements in JT-60SA

K. Tanaka,^{1,2,a)} S. Coda,³ M. Yoshida,⁴ H. Sasao,⁴ Y. Kawano,⁴ R. Imazawa,⁴ H. Kubo,⁴ and Y. Kamada⁴

¹National Institute for Fusion Science, Toki, Gifu 509-5292, Japan

²Department of Advanced Energy Engineering, Kyushu University, Kasuga, Fukuoka 816-8580, Japan

³EPFL-SPC, Lausanne, Switzerland

⁴National Institutes for Quantum and Radiological Science and Technology, Naka, Ibaraki 311-0193, Japan

(Presented 7 June 2016; received 5 June 2016; accepted 5 July 2016;

published online 16 August 2016)

A tangential viewing phase contrast imaging system is being designed for the JT-60SA tokamak to investigate microturbulence. In order to obtain localized information on the turbulence, a spatial-filtering technique is applied, based on magnetic shearing. The tangential viewing geometry enhances the radial localization. The probing laser beam is injected tangentially and traverses the entire plasma region including both low and high field sides. The spatial resolution for an Internal Transport Barrier discharge is estimated at 30%–70% of the minor radius at $k = 5 \text{ cm}^{-1}$, which is the typical expected wave number of ion scale turbulence such as ion temperature gradient/trapped electron mode. *Published by AIP Publishing.* [<http://dx.doi.org/10.1063/1.4960057>]

I. INTRODUCTION

This paper describes the conceptual design study of a tangential phase contrast imaging (T-PCI) diagnostic for JT-60SA¹ to measure microturbulence. JT-60SA is a superconducting tokamak, which will start operation in 2019. JT-60SA will cover an operational range of normalized collisionality, normalized beta, and normalized ion Larmor radius relevant to both ITER and DEMO.

The investigation of microturbulence is one of the most important areas of magnetic fusion research. Turbulence plays a crucial role in all transport channels such as energy, particle, impurity, and momentum. While simulation studies based on gyrokinetic and gyrofluid turbulence modeling are widely performed, simulation validation through turbulence measurements is limited. This is due in part to the difficulty of measurements of turbulence. In the last two decades, microwave reflectometry² and beam emission spectroscopy (BES) have arguably been the most common techniques. Reflectometry can measure turbulence with very fine resolution, down to 1% of the minor radius. However, the measurement location depends on plasma density and on the magnetic field profile. Reflectometry is very suitable for measuring edge turbulence, where the density gradient is steep. BES is a powerful technique that can generate a direct two dimensional picture of the turbulence.³ BES can measure core turbulence when a heating or diagnostic neutral beam is available and the signal is strong enough. A fine spatial resolution (1%~10% of minor radius) is possible when the viewing geometry is optimized. Both microwave reflectometry and BES are being planned for JT-60SA.¹

Compared with microwave reflectometry and BES, PCI has the advantage of unrestricted applicability. Operation is not limited by any plasma condition or heating scheme. Also, PCI has good access to core turbulence, which is appropriate for comparisons with gyrokinetic and gyrofluid simulations. Phase contrast imaging is a laser-based homodyne scattering technique that is very sensitive to small amplitude turbulence. Given the 90° phase difference to first order between scattered and un-scattered components, the small phase variations due to the change in refractive index caused by electron density fluctuations can be converted into measurable intensity variations by changing that phase difference with a spatial filter. The image of the turbulence is then projected onto the detection plane. However, due to the large scattering volume, in the basic PCI technique, the measurement is line integrated. In order to obtain a local image of the turbulence, an additional selection technique based on magnetic shear is necessary, which is used in LHD,^{4,5} TCV,^{6,7} and DIII-D.⁸ This technique makes use of the strong asymmetry of the turbulence and magnetic shear. This is described in Section II.

In PCI, the minimum measurable k is determined by beam width, while the maximum measurable k is determined by the spacing of the detector array and size of the collection optics. The k dynamic range can be enhanced by adjusting the magnification. Usually, the infrared region around 10 μm is used for PCI. This is because stable and powerful CO₂ lasers and highly sensitive semiconductor detector arrays are available in this wavelength region.

II. PRINCIPLE OF PCI WITH MAGNETIC SHEAR TECHNIQUE AND SYSTEM DESCRIPTION

Figure 1 shows the principle of the magnetic shear technique. The magnetic shear technique was first applied to PCI in Heliotron E.⁹ The wavelength of the turbulence in

Note: Contributed paper, published as part of the Proceedings of the 21st Topical Conference on High-Temperature Plasma Diagnostics, Madison, Wisconsin, USA, June 2016.

^{a)}Electronic mail: ktanaka@nifs.ac.jp.

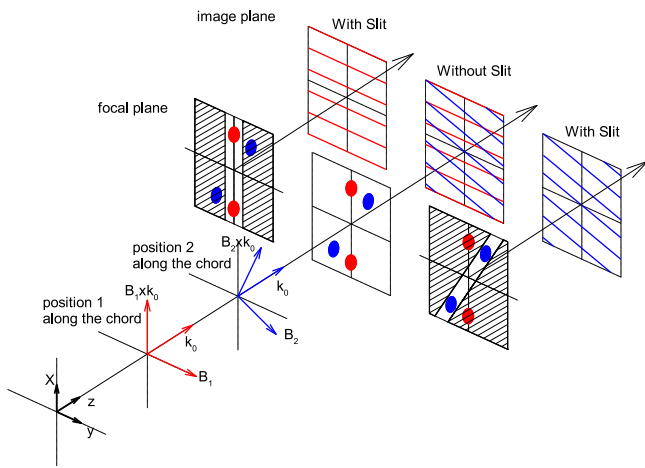


FIG. 1. Principle of magnetic shear technique. k_0 is the wavenumber vector of injected laser beam and B_1, B_2 are the vector of magnetic field at position 1 and 2. Measured wavenumber components are $B_1 \times k_0$ and $B_2 \times k_0$.

the magnetized plasma perpendicular to the magnetic field is of the order of the electron or ion Larmor radius, while the wavelength parallel to the magnetic field is of the order of the connection length, i.e., much longer. This restricts the detectable wave vector to one direction at each spatial point, which twists in space due to the twisting of the magnetic field. As a result, the scattered components focus at different positions on the focal plane (Fourier plane) and have different propagation directions in the image plane, as shown in Fig. 1. In TCV and DIII-D, the wave vector direction is selected with slits, and the turbulence is measured by 1D detector arrays.⁶⁻⁸ In LHD, a two dimensional image of the fluctuations is measured by a 2D detector array, and the location selection occurs by digital spatial Fourier transform.^{4,5,10} For an equal number of pixels, the 1D slit technique has better k resolution and dynamic range and the spatial profile of the turbulence can be obtained by rotating the slit between shots or dynamically in the steady state phase of the discharge. The maximum entropy method is suitable to get the 2D k spectrum from a limited number of pixels.¹⁰ Using the 2D technique, the complete spatial profile of the turbulence is obtained at each instant.

The magnetic shear technique works best for large variations of the projected field angle (the precession of the magnetic field around the laser beam). This is the case for LHD with a vertical view,⁴ for which the projected field angle changes by $\pm 50^\circ$. In a conventional tokamak, however, the angle variation is about $\pm 10^\circ$ for a vertical view. On the other hand, in a tokamak a tangential view yields a large variation of the projected field angle, so that spatial resolution is dramatically improved.⁶ In general, the region of near-tangency to the magnetic field offers the best localization.

Figure 2 shows the beam path of the system. The CO₂ laser beam is transmitted from the laser room to the torus main hall. Then, the beam is injected tangentially. After passing through the vacuum vessel, the beam goes to the detection box. A CO₂ laser two color interferometer for electron density measurements is planned for the same port section but a different port window with a double pass arrangement.^{1,11} The two CO₂ laser diagnostics do not interfere with each other.

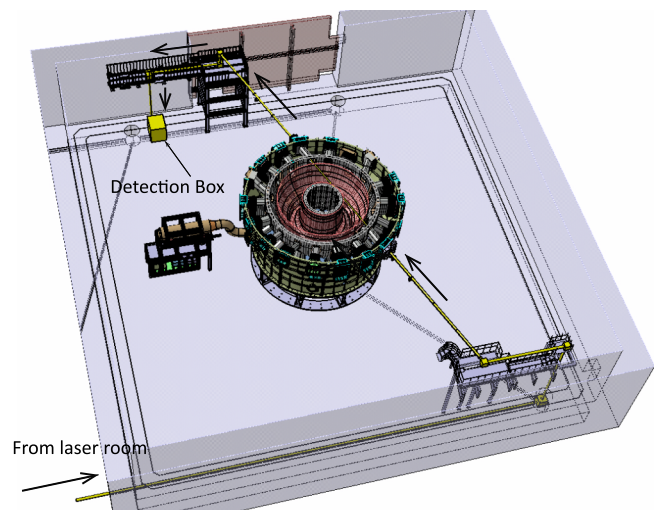


FIG. 2. Design of beam transmission of JT-60SA T-PCI.

Figure 3 shows a schematic view of the detection system as currently envisioned. The laser beam is focused on the groove of the phase plate, which introduces a 90° phase difference between scattered and unscattered components. The groove of the phase plate will be coated to attenuate the unscattered components in order to prevent detector saturation and enhance the contrast. The beam is feedback controlled to keep the focusing spot on the groove of phase plate. This technique was already developed for DIII-D⁸ and TCV.^{6,7} The beam is envisioned to be split and sent to the 1D and 2D detection areas. The 1D detection system measures a wide k range of fluctuations. A remotely controlled rotating slit selects the location of interest as shown in Fig. 1. The 2D detection system measures the entire fluctuation profile simultaneously as illustrated in Fig. 1 (case without slit). L1 is located at the first image plane and adjusts the beam width. The three-lens arrangements allow varying the magnification in order to vary the k dynamic range. The detector will likely be a liquid nitrogen cooled Mercury Cadmium Telluride (MCT) semiconductor detector. Cooling is necessary to minimize the thermal noise and detect weak signals. The 2D system may use a photoconductive (PC) type and the 1D system a photovoltaic (PV) type, as the former's typical bandwidth (~ 2 MHz) can cover the ion temperature gradient (ITG)/trapped electron mode (TEM) region, while the latter can extend to higher frequencies and cover the electron temperature gradient (ETG) region.

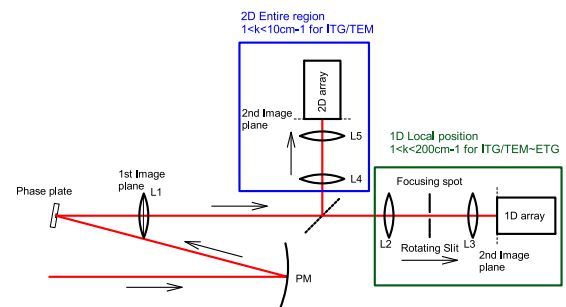


FIG. 3. Detection system.

In JT-60SA, deuterium gas and deuterium neutral beams will be used from the second initial research phase.¹ Therefore, semiconductor devices such as MCT detectors, amplifiers, and the beam feedback control system should be protected against neutron and gamma ray irradiation. The expected fluence is now being calculated to design the shielding. Approximately 12 cm thick borated polyethylene to reduce the 2.45 MeV D-D neutron fluence by one order of magnitude and 1 cm thick lead plate to reduce gamma ray fluence about a factor of three will likely be necessary. The system should be one week maintenance free. The liquid nitrogen should be fueled automatically. Shielding and a liquid nitrogen fueling system are now under development for LHD deuterium experiments. The experience in LHD will be used to design the JT-60SA system.

III. GEOMETRY AND SPATIAL RESOLUTION

The achievable spatial resolution has been estimated for the equilibrium of an Internal Transport Barrier (ITB) discharge in JT-60SA. The beam path in the vessel is for the present available port as shown in Fig. 2. Figure 4(a) shows a top view of beam transmission. The beam is injected tangentially and horizontally. In TCV, the tangency point is close to the magnetic axis and the rapid projected angle variation there yields a spatial resolution down to 1% of the minor radius. However, presently, such a view is not available in JT-60SA. The tangent radius is 1.755 m and is inside the inner boundary. As shown in Figs. 4(a) and 4(b), the beam traverses the entire minor radius four times, twice on the low and twice on the high field side. The measured k is predominantly poloidal close to the edge and radial close to the plasma center. This enables the investigation of ballooning effects on turbulence and possibly toroidal correlation. Figure 4(c) shows the variation of the projected magnetic field angle onto the detection plane, which is perpendicular to the beam axis. The angle varies by around $\pm 40^\circ$ as shown in Fig. 4(c). This is almost comparable with the

LHD vertical view, for which the angle variation is $\pm 50^\circ$.⁴ In contrast to JT-60SA, the beam traverses the entire minor radius only twice in the LHD PCI system.⁴

Spatial resolution is calculated as follows. As shown in Fig. 1, scattered components are focused at different positions in the two dimensional focal plane. A slit can select particular scattered components. We consider a diffraction-limited system, i.e., an optimal slit with a width equal to the width of the focal spot. The corresponding angular resolution, defined as the $1/e^2$ width, yields the spatial resolution through the curves of Fig. 4(c). The focal spot is a crucial parameter, a smaller one yielding better spatial resolution, and requiring a larger beam width in the plasma. Presently, the designed beam width defined by $1/e^2$ intensity is 10 cm. The window and mirror sizes are large enough for the probe beam and scattered components. Figure 4(d) shows the calculated spatial resolution along the beam path for $k = 2-20 \text{ cm}^{-1}$.

Better spatial resolution is achieved on the low field side. According to a gyrokinetic linear calculation for a JT-60U discharge,¹² the unstable region at $\rho = 0.25$ is $k\rho_i = 0.1-1$, where k is the poloidal wavenumber and ρ_i is the ion Larmor radius; $k\rho_i = 0.1-50$ at $\rho = 0.5$ and $k\rho_i = 0.1-100$ at $\rho = 0.75$. Typical parameters for a deuterium discharge of JT-60SA will be $T_i = 1-10 \text{ keV}$ and $B_t = 2.25 \text{ T}$. This corresponds to $\rho_i = 0.2-0.64 \text{ cm}$. The dominant part of ion scale turbulence such as ITG and TEM typically occupies $k\rho_i = 0.1-2$, i.e., $k < 5 \text{ cm}^{-1}$. Table I shows a summary of the spatial resolution for $k = 2-10 \text{ cm}^{-1}$. From the experience in LHD, TCV, and DIII-D, it is thus promising to measure ion scale turbulence such as ITG/TEM using PC type MCT. As shown in Table I, at $k = 5 \text{ cm}^{-1}$ the spatial resolution is 30%-70% of the minor radius. This spatial resolution is sufficient to investigate the correlation between ion scale turbulence and transport. Also, synthetic diagnostics¹³ will help to understand the turbulence characteristics. Far better spatial resolution

TABLE I. Summary of spatial resolution for ITB discharge.

High field side				Low field side			
$R_{\min} = 1.755 \text{ m at } \rho = -0.25$				$R_{\min} = 1.755 \text{ m at } \rho = 0.25$			
$k \text{ (cm}^{-1}\text{)}$	$k\rho_i \text{ min}$	$k\rho_i \text{ max}$	$\delta\rho$	$k \text{ (cm}^{-1}\text{)}$	$k\rho_i \text{ min}$	$k\rho_i \text{ max}$	$\delta\rho$
2.00	0.40	1.28	0.86	2.00	0.40	1.28	0.44
5.00	1.00	3.20	0.34	5.00	1.00	3.20	0.27
10.00	2.00	6.40	0.18	10.00	2.00	6.40	0.15
$R_{\min} = 1.755 \text{ m at } \rho = -0.5$				$R_{\min} = 1.755 \text{ m at } \rho = 0.5$			
$k \text{ (cm}^{-1}\text{)}$	$k\rho_i \text{ min}$	$k\rho_i \text{ max}$	$\delta\rho$	$k \text{ (cm}^{-1}\text{)}$	$k\rho_i \text{ min}$	$k\rho_i \text{ max}$	$\delta\rho$
2.00	0.40	1.28	0.90	2.00	0.40	1.28	0.79
5.00	1.00	3.20	0.65	5.00	1.00	3.20	0.29
10.00	2.00	6.40	0.20	10.00	2.00	6.40	0.14
$R_{\min} = 1.755 \text{ m at } \rho = -0.75$				$R_{\min} = 1.755 \text{ m at } \rho = 0.75$			
$k \text{ (cm}^{-1}\text{)}$	$k\rho_i \text{ min}$	$k\rho_i \text{ max}$	$\delta\rho$	$k \text{ (cm}^{-1}\text{)}$	$k\rho_i \text{ min}$	$k\rho_i \text{ max}$	$\delta\rho$
2.00	0.40	1.28	0.84	2.00	0.40	1.28	0.64
5.00	1.00	3.20	0.55	5.00	1.00	3.20	0.47
10.00	2.00	6.40	0.42	10.00	2.00	6.40	0.37

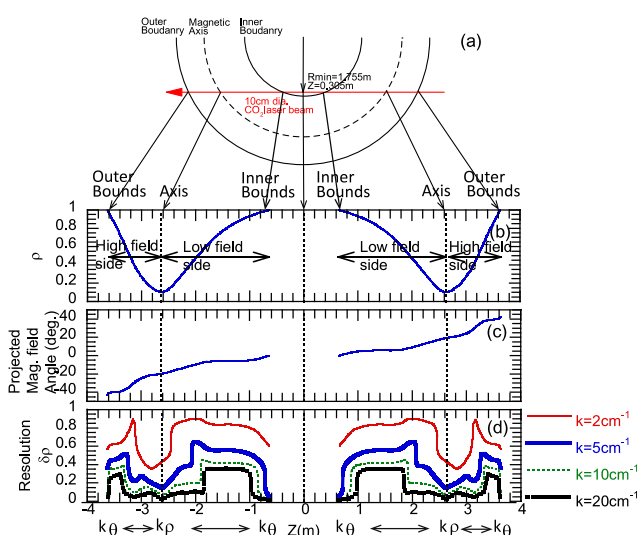


FIG. 4. Spatial resolution of T-PCI in JT-60SA. (a) Schematic view of the beam path, (b) normalized position along the beam, (c) projected magnetic field angle, and (d) spatial resolution. Z coordinate is along beam axis.

is obtained for higher k , but in this case, increase of the phase contrast and use of a PV type detector are likely to be essential.

- ¹See http://www.jt60sa.org/b/index_nav_3.htm?n3/operation.htm for JT-60SA Research Plan Version 3.3.
- ²E. Mazzucato, *Rev. Sci. Instrum.* **69**, 2201 (1998).
- ³G. R. Mckee, R. J. Fonck, D. K. Gupta, D. J. Schlossberg, M. W. Shafer, R. L. Boivin, and W. Solomon, *Plasma Fusion Res.* **2**, S1025 (2007).
- ⁴K. Tanaka, C. A. Michael, L. N. Vyacheslavov, A. L. Sanin, K. Kawahata, T. Akiyama, T. Tokuzawa, and S. Okajima, *Rev. Sci. Instrum.* **79**, 10E702 (2008).
- ⁵K. Tanaka, C. A. Michael, L. N. Vyacheslavov *et al.*, *Plasma Fusion Res.* **5**, S2052 (2010).

- ⁶A. Marinoni, S. Coda, R. Chavan, and G. Pochon, *Rev. Sci. Instrum.* **77**, 10E929 (2006).
- ⁷Z. Huang, S. Coda, and C. A. de Meijere, in Proceeding of EPS Conference, Germany, Berlin, 23–27 June 2014.
- ⁸J. R. Dorris, J. C. Rost, and M. Porkolab, *Rev. Sci. Instrum.* **80**, 023503 (2009).
- ⁹S. Kado, T. Irie, K. Muraoka, K. Matsuo, K. Tanaka, K. Kondo, F. Sano, and T. Obiki, *Jpn. J. Appl. Phys., Part 1* **34**, 6492 (1995).
- ¹⁰C. A. Michael, K. Tanaka, L. Vyacheslavov, A. Sanin, and K. Kawahata, *Rev. Sci. Instrum.* **86**, 093503 (2015).
- ¹¹H. Sasao, Y. Kawano, H. Arakawa, T. Sakuma, R. Imazawa, H. Kubo, and K. Itami, *J. Instrum.* **11**, C02082 (2016).
- ¹²M. Nakata, M. Honda, M. Yoshida, H. Urano, M. Nunami, S. Maeyama, T. H. Watanabe, and H. Sugama, *Nucl. Fusion* **56**, 086010 (2016).
- ¹³J. C. Rost, L. Lin, and M. Porkolab, *Phys. Plasmas* **17**, 062506 (2010).